2-Picolinate Decorated Iron–Lanthanide Heterometallic Germanotungstates Including an S-shaped $[Ge_2W_{20}O_{72}]^{16-}$ Segment

Jun Jiang, Yanhong Chen, Lulu Liu, Lijuan Chen* and Junwei Zhao*

Henan Key Laboratory of Polyoxometalate Chemistry, College of Chemistry and Chemical Engineering, Henan University, Kaifeng, Henan 475004, People's Republic of China. *E-mail: ljchen@henu.edu.cn, zhaojunwei@henu.edu.cn

Supporting Information

Figure S1. Comparison of PXRD patterns for **1** (a), **3** (b), **4** (c), **6** (d), **7** (e) and **10** (f) with simulated X-ray diffraction patterns from single-crystal structural analyses.

Figure S2. (a) Polyoxoanionic skeleton for **10**. (b-d) Coordination spheres of $Eu1^{3+}$, $Fe1^{3+}$ and $Fe2^{3+}$ ions in **10**.

Figure S3. (a) Space packing for **1** with a regular –ABAB– fashion in ab plane. (b) Simplified packing for **1**. (c) Layer A in bc plane. (d) Simplified layer A. (e) Layer B in bc plane. (f) Simplified layer B. (g-h) Representations of 3D stacking for **1** in bc plane. (i) Simplified 3D stacking for **1** in bc plane.

Figure S4. (a) Space packing for **10** with a regular –ABAB–fashion in ab plane. (b) Simplified packing for **10**. (c) Layer A in bc plane. (d) Simplified layer A. (e) Layer B in bc plane. (f) Simplified layer B. (g-h) Representations of 3D stacking for **10** in bc plane. (i) Simplified 3D stacking for **10** in bc plane.

Figure S5. Solid-state excitation spectrum for **3** (λ_{em} = 1056 nm) at room temperature.

Figure S6. Solid-state excitation spectrum for **4** (λ_{em} = 642 nm) at room temperature.

Figure S7. Solid-state excitation spectrum for **6** (λ_{em} = 543 nm) at room temperature.

Figure S8. Solid-state excitation spectrum for **10** (λ_{em} = 616 nm) at room temperature.

Figure S9. (a) Solid-state emission spectrum for $K_8[\gamma\text{-}GeW_{10}O_{36}]\cdot 6H_2O$ (λ_{ex} = 403 nm) at room temperature. (b) Luminescence decay profile for $K_8[\gamma\text{-}GeW_{10}O_{36}]\cdot 6H_2O$ taken through supervising 470 nm emission.

Figure S10. (a) Solid-state emission spectrum for $K_8[\gamma\text{-}GeW_{10}O_{36}]\cdot 6H_2O$ (λ_{ex} = 379 nm) at room temperature. (b) Luminescence decay profile for $K_8[\gamma\text{-}GeW_{10}O_{36}]\cdot 6H_2O$ taken through supervising 470 nm emission.

Figure S11. (a) Solid-state emission spectrum for $K_8[\gamma\text{-}GeW_{10}O_{36}]\cdot 6H_2O$ (λ_{ex} = 464 nm) at room temperature. (b) Luminescence decay profile for $K_8[\gamma\text{-}GeW_{10}O_{36}]\cdot 6H_2O$ taken through supervising 530 nm emission.

Figure S12. (a) Solid-state emission spectra for $K_8[\gamma\text{-}GeW_{10}O_{36}]\cdot 6H_2O$ (λ_{ex} = 265 nm) at room temperature. (b) Solid-state excitation spectrum for $K_8[\gamma\text{-}GeW_{10}O_{36}]\cdot 6H_2O$ (λ_{ex} = 520 nm) at room temperature. (c) Solid-state emission spectrum for Hpic ligand (λ_{ex} = 265 nm) at room temperature.

Figure S13. Excitation spectrogram for **10** (λ_{em} = 616 nm).

Materials and methods. All chemicals were commercially purchased and used without further purification. $K_8Na_2[A\text{-}\alpha\text{-}GeW_9O_{34}]\cdot 25H_2O$ and $K_8[\gamma\text{-}GeW_{10}O_{36}]\cdot 6H_2O$ were synthesized as described in the previous literature,[1-3] and characterized by IR spectra. Elemental analyses (carbon, hydrogen and nitrogen) were performed on a Vario EL Cube CHNS analyzer. IR spectra were received from a solid sample palletized with KBr on a Nicolet 170 SXFT-IR spectrometer in the range 400–4000 cm^{-1}. PXRD measurements were taken by a Bruker D8 ADVANCE apparatus with Cu Kα radiation (λ = 1.54056 Å) at 293 K. TG analyses were performed under a N_2 atmosphere on a Mettler-Toledo TGA/SDTA 851^e instrument with a heating rate of 10 °C min^{-1} from 25 to 800 °C. Photoluminescence spectra and lifetimes were recorded using an FLS 980 Edinburgh Analytical Instrument apparatus equipped with a 450 W xenon lamp and a μF900H high energy microsecond flashlamp as the excitation sources. Magnetic measurements were carried out with a Quantum Design MPMS-XL-7 magnetometer in the temperature range of 2–300 K.

Preparation of $[La(H_2O)_8]_2H_2[Fe_4(H_2O)_4(pic)_4Ge_2W_{20}O_{72}]\cdot 34H_2O$ (1). A mixture of $K_8Na_2[A\text{-}\alpha\text{-}GeW_9O_{34}]\cdot 25H_2O$ (1.001 g, 0.621 mmol), $La(NO_3)_3\cdot 6H_2O$ (0.087 g, 0.201 mmol), Hpic (0.125 g, 1.015 mmol) and 10 mL of distilled water was stirred for 0.5 h. The pH value of this system was adjusted to 2.3 using 2 M hydrochloric acid. After stirring for another 0.5 h, $FeCl_3\cdot 6H2O$ (0.108g, 0.398 mmol) was added in the mixture, and the pH value at this moment is about 1.2. The reaction mixture was continuously stirred for 0.5 h and sealed in a 25 mL Teflon-lined steel autoclave, kept at 80 °C for 5 d. Then the mixture was cooled to room temperature and yellow block crystals were gathered by filtering, washed with distilled water and dried in air at ambient temperature. Yield: ca. 0.22 g (7.89 %) based on $La(NO_3)_3\cdot 6H_2O$. Elemental analysis (%) calcd: C, 4.15; H, 1.83; N, 0.81; W, 52.99; Ge, 2.09; Fe, 3.22; La, 4.00. Found: C, 4.35; H, 1.93; N, 0.71; W, 52.78; Ge, 1.84; Fe, 3.37; La, 4.18. IR (KBr, cm^{-1}): 3426 (s), 1636 (s), 1602 (s), 1477(w), 1369(m), 1297(w), 948 (s), 806 (s), 695 (m), 648 (m) (Figure S17).

Preparation of $[Ce(H_2O)_8]_2H_2[Fe_4(H_2O)_4(pic)_4Ge_2W_{20}O_{72}]\cdot 34H_2O$ (2). The synthetic procedure of **2** is similar to **1** except that $La(NO_3)_3\cdot 6H_2O$ was replaced by $Ce(NO_3)_3\cdot 6H_2O$ (0.084 g, 0.193 mmol). Yellow block crystals of 2 were obtained. Yield: ca. 0.18 g (6.72 %) based on $Ce(NO_3)_3\cdot 6H_2O$. Elemental analysis (%) calcd: C, 4.15; H, 1.83; N, 0.81; W, 52.97; Ge, 2.09; Fe, 3.22; Ce, 4.04. Found: C, 4.40; H, 1.95; N, 0.66, W, 52.70; Ge, 1.80; Fe, 3.32; Ce, 4.12. IR (KBr, cm^{-1}): 3433 (s), 1632 (s), 1601 (s), 1474(w), 1374(m), 1295(w), 948 (s), 806 (s), 701 (m), 643 (m) (Figure S17).

Preparation of $[Nd(H_2O)_8]_2H_2[Fe_4(H_2O)_4(pic)_4Ge_2W_{20}O_{72}]\cdot 34H_2O$ (3). The synthetic procedure of **3** is similar to **1** except that $La(NO_3)_3\cdot 6H_2O$ was replaced by $Nd(NO_3)_3\cdot 6H_2O$ (0.085 g, 0.194 mmol). Yellow block crystals of **3** were obtained. Yield: 0.25 g (9.72 %) based on $Nd(NO_3)_3\cdot 6H_2O$. Elemental analysis (%) calcd: C, 4.15; H, 1.83; N, 0.81; W, 52.91; Ge, 2.09; Fe, 3.21; Nd, 4.15. Found: C, 4.31; H, 1.89; N, 0.70, W, 52.72; Ge, 1.89; Fe, 3.35; Nd, 4.30. IR (KBr, cm^{-1}): 3343 (s), 1632 (s), 1601 (s), 1474(w), 1374(m), 1295(w), 953 (s), 806 (s), 695 (m), 648 (m) (Figure S17).

Preparation of $[Sm(H_2O)_8]_2H_2[Fe_4(H_2O)_4(pic)_4Ge_2W_{20}O_{72}]\cdot 34H_2O$ (4). The synthetic procedure of **4** is similar to **1** except that $La(NO_3)_3\cdot 6H_2O$ was replaced by $Sm(NO_3)_3\cdot 6H_2O$ (0.087 g, 0.196 mmol). Yellow block crystals of **4** were obtained. Yield: 0.38 g (13.93 %) based on $Sm(NO_3)_3\cdot 6H_2O$. Elemental analysis (%) calcd: C, 4.14; H, 1.82; N, 0.80; W, 52.82; Ge, 2.09; Fe, 3.21; Sm, 4.32. Found: C, 4.37 H, 1.86; N, 0.66, W, 52.65; Ge, 1.93; Fe, 3.37; Sm, 4.22. IR (KBr, cm^{-1}): 3396 (s), 1638 (s), 1601 (s), 1480(w), 1369(m), 1295(w), 948 (s), 801 (s), 695 (m), 643 (m) (Figure S17).

Preparation of $[Gd(H_2O)_8]_2H_2[Fe_4(H_2O)_4(pic)_4Ge_2W_{20}O_{72}]\cdot 34H_2O$ (5). The synthetic procedure of **5** is similar to **1** except that $La(NO_3)_3\cdot 6H_2O$ was replaced by $Gd(NO_3)_3\cdot 6H_2O$ (0.084 g, 0.188 mmol). Yellow block crystals of **5**

were obtained. Yield: 0.32 g (12.2 %) based on $Gd(NO_3)_3·6H_2O$. Elemental analysis (%) calcd: C, 4.13; H, 1.82; N, 0.80; W, 52.71; Ge, 2.08; Fe, 3.20; Gd, 4.51. Found: C, 4.29; H, 1.90; N, 0.70, W, 52.59; Ge, 1.89; Fe, 3.41; Gd, 4.38. IR (KBr, cm^{-1}): 3480 (s), 1638 (s), 1601 (s), 1474(w), 1369(m), 1295(w), 953 (s), 801 (s), 695 (m), 643 (m) (Figure S17).

Preparation of $[Tb(H_2O)_8]_2H_2[Fe_4(H_2O)_4(pic)_4Ge_2W_{20}O_{72}]·34H_2O$ (6). The synthetic procedure of **6** is similar to **1** except that $La(NO_3)_3·6H_2O$ was replaced by $Tb(NO_3)_3·6H_2O$ (0.086 g, 0.188 mmol). Yellow block crystals of 6 were obtained. Yield: 0.43 g (16.39 %) based on $Tb(NO_3)_3·6H_2O$. Elemental analysis (%) calcd: C, 4.13; H, 1.82; N, 0.80; W, 52.69; Ge, 2.08; Fe, 3.20; Tb, 4.55. Found: C, 4.33; H, 1.87; N, 0.65, W, 52.53; Ge, 1.84; Fe, 3.27; Tb, 4.46. IR (KBr, cm^{-1}): 3380 (s), 1632 (s), 1601 (s), 1474(w), 1404(m), 1295(w), 953 (s), 806 (s), 695 (m), 643 (m) (Figure S17).

Preparation of $[Dy(H_2O)_8]_2H_2[Fe_4(H_2O)_4(pic)_4Ge_2W_{20}O_{72}]·34H_2O$ (7). The synthetic procedure of **7** is similar to **1** except that $La(NO_3)_3·6H_2O$ was replaced by $Dy(NO_3)_3·6H_2O$ (0.087 g, 0.188 mmol). Yellow block crystals of **7** were obtained. Yield: 0.28 g (10.66 %) based on $Dy(NO_3)_3·6H_2O$. Elemental analysis (%) calcd: C, 4.13; H, 1.82; N, 0.80; W, 52.63; Ge, 2.08; Fe, 3.20; Dy, 4.65. Found: C, 4.29; H, 1.93; N, 0.69, W, 52.60; Ge, 1.90; Fe, 3.33; Dy, 4.44. IR (KBr, cm^{-1}): 3417 (s), 1632 (s), 1601 (s), 1480(w), 1389(m), 1295(w), 953 (s), 806 (s), 701 (m), 643 (m) (Figure S17).

Preparation of $[Er(H_2O)_8]_2H_2[Fe_4(H2O)_4(pic)_4Ge_2W_{20}O_{72}]·34H_2O$ (8). The synthetic procedure of **8** is similar to **1** except that $La(NO_3)_3·6H_2O$ was replaced by $Er(NO_3)_3·6H_2O$ (0.065 g, 0.141 mmol). Yellow block crystals of **8** were obtained. Yield: 0.42 g (21.27 %) based on $Er(NO_3)_3·6H_2O$. Elemental analysis (%) calcd: C, 4.12; H, 1.82; N, 0.80; W, 52.56; Ge, 2.07; Fe, 3.19; Er, 4.78. Found: C, 4.26; H, 1.99; N, 0.62, W, 52.44; Ge,1.87; Fe, 3.31; Er, 4.55. IR (KBr, cm^{-1}): 3389 (s), 1633 (s), 1597 (s), 1476(w), 1374(m), 1295(w), 955 (s), 802 (s), 701 (m), 640 (m) (Figure S17).

Preparation of $[Tm(H_2O)_8]_2H_2[Fe_4(H2O)_4(pic)_4Ge_2W_{20}O_{72}]·34H_2O$ (9). The synthetic procedure of **9** is similar to **1** except that $La(NO_3)_3·6H_2O$ was replaced by $Tm(NO_3)_3·6H_2O$ (0.065 g, 0.140 mmol). Yellow block crystals of **9** were obtained. Yield: 0.33 g (16.84 %) based on $Tm(NO_3)_3·6H_2O$. Elemental analysis (%) calcd: C, 4.12; H, 1.81; N, 0.80; W, 52.54; Ge, 2.08; Fe, 3.19; Tm, 4.83. Found: C, 4.33; H, 1.94; N, 0.72, W, 52.44; Ge, 1.93; Fe, 3.27; Tm, 4.69. IR (KBr, cm^{-1}): 3359 (s), 1633 (s), 1600 (s), 1478(w), 1374(m), 1295(w), 952 (s), 799 (s), 701 (m), 640 (m) (Figure S17).

Preparation of $[Eu(H_2O)_8]_2H_2[Fe_4(H2O)_4(pic)_4Ge_2W_{20}O_{72}]·36H_2O$ (10). The synthetic procedure of **10** is similar to **1** except that $La(NO_3)_3·6H_2O$ was replaced by $Eu(NO_3)_3·6H_2O$ (0.085 g, 0.190 mmol). Yellow block crystals of **10** were obtained. Yield: 0.40 g (24.1 %) based on $Eu(NO_3)_3·6H_2O$. Elemental analysis (%) calcd: C, 4.12; H, 1.87; N, 0.80; W, 52.52; Ge, 2.08; Fe, 3.19; Eu, 4.34. Found: C, 4.36; H, 1.94; N, 0.77, W, 52.61; Ge, 1.89; Fe, 3.06; Eu, 4.26. IR (KBr, cm^{-1}): 3359 (s), 1632 (s), 1598 (s), 1480(w), 1387(m), 1297(w), 954 (s), 807 (s), 701 (m), 644 (m) (Figure S17).

X-ray crystallography. Single-crystal X-ray diffraction data of **1–10** were collected on a Bruker APEX–II CCD detector at 150 K with Mo Kα radiation (λ = 0.71073 Å). Direct methods were used to solve their structures and locate the heavy atoms using the SHELXTL-97 program package. The remaining atoms were found from successive full-matrix least-squares refinements on F^2 and Fourier syntheses. Lorentz polarization and SADABS corrections were applied.[4] All hydrogen atoms attached to carbon and nitrogen atoms were geometrically placed and refined isotropically as a riding model using the default SHELXTL parameters.[5-6] No hydrogen atoms associated with water molecules were located from the difference Fourier map. All non-hydrogen atoms were refined anisotropically. In the refinement of **1–9**, eight lattice water molecules per molecule of **1–9** and eighteen lattice water molecules per molecule of **10** were found from the Fourier maps. However, there are still solvent accessible voids accessible solvent

voids in the check cif reports of crystal structures, suggesting that some water molecules should exist in the structures, which can't be found from the weak residual electron peaks. These water molecules are highly disordered and attempts to locate and refine them were unsuccessful. The SQUEEZE program performed in PLATON was further used to calculate and evaluate the possible numbers of the disordered solvent water molecules in the accessible voids of their crystal structures. Based on the electron count and void volume, twenty-six water molecules were directly added to each molecular formula of **1–9** in the revised paper. Similarly, eighteen water molecules were directly added to each molecular formula of **10** in the revised paper, which are basically consistent with the results of elemental analyses and TG analyses**.** The crystallographic data and structure refinement parameters for **1–10** are demonstrated in Table S1. Crystallographic data and structure refinements for **1–10** reported in this paper have been deposited in the Cambridge Crystallographic Data Centre with CCDC 1941771–1941777, 1955082-1955083, 1941778. These data can be obtained free of charge from the Cambridge Crystallographic Data Centre via www.ccdc.cam.ac.uk/data_request/cif.

1 Haraguchi N.; Okaue Y.; Isobe T.; Matsuda Y.; Stabilization of Tetravalent Cerium upon Coordination of Unsaturated Heteropolytungstate Anions, *Inorg. Chem.* **1994**, *33*, 1015–1020.

2 Bi L. H.; Kortz U.; Nellutla S.; Stowe A. C.; Tol J. v.; Dalal N. S.; Structure, electrochemistry, and magnetism of the Iron(III)-substituted Keggin dimer, $[Fe_6(OH)_3(A\text{-}\alpha\text{-}GeW_9O_{34}(OH)_3)_2]^{11-}$. *Inorg. Chem.* **2005**, *44*, 896–903.

3 Nsouli N. H.; Bassil B. S.; Dickman M. H.; Kortz U.; Keita B.; Nadjo L. Synthesis and structure of dilacunary decatungstogermanate, $[\gamma\text{-}GeW_{10}O_{36}]^{8-}$. *Inorg. Chem.* **2006**, *45*, 3858–3860.

4 Sheldrick, G. M. SADABS: Program for Empirical Absorption Correction of Area Detector Data, University of Göttingen: Göttingen, Germany, 1996.

5 Sheldrick, G. M. SHELXL97, Program for Crystal Structure Refinement; University of Göttingen: Göttingen, Germany, 1997.

6 Sheldrick, G. M. SHELXS97, Program for Crystal Structure Solution; University of Göttingen: Göttingen, Germany, 1997.

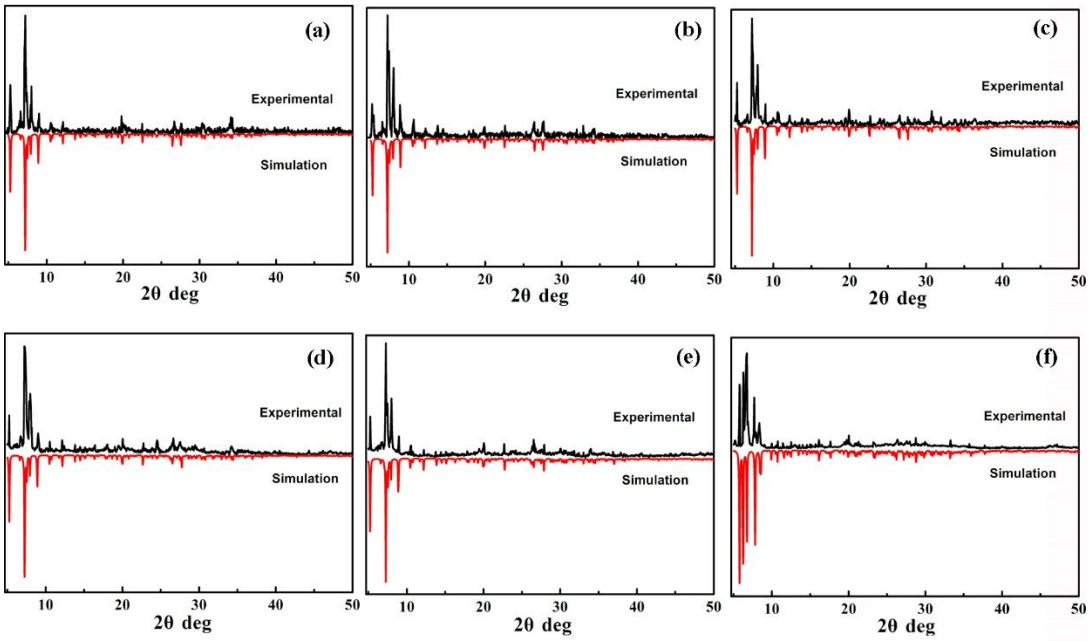

Figure S1. Comparison of PXRD patterns for **1** (a), **3** (b), **4** (c), **6** (d), **7** (e) and **10** (f) with simulated X-ray diffraction patterns from single-crystal structural analyses.

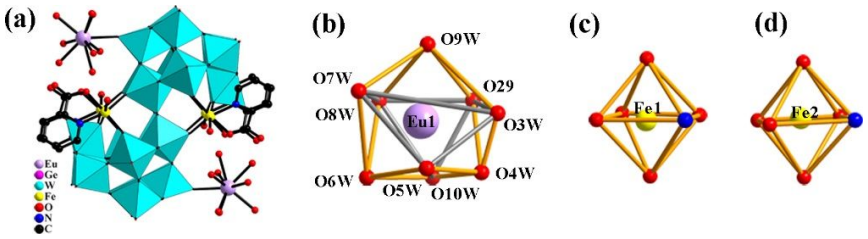

Figure S2. (a) Polyoxoanionic skeleton for **10**. (b-d) Coordination spheres of $Eu1^{3+}$, $Fe1^{3+}$ and $Fe2^{3+}$ ions in **10**.

In $Eu1^{3+}$ coordination polyhedron in **10**, three side faces of the triangular prism are constituted by the O8W–O7W–O5W–O10W, O5W–O10W–O29–O3W, and O8W–O7W–O3W–O29 groups with standard deviations of 0.0926 Å, 0.3052 Å and 0.1336 Å from their least-square planes, and the dihedral angles between adjacent side faces are 81.2°, 44.8° and 55.0°. The distance between the $Eu1^{3+}$ ion and the above-mentioned three side faces are 0.7963 Å, 1.2589 Å and 0.6336 Å, respectively. O6W, O4W, and O9W are located at the three cap positions over O8W–O7W–O5W–O10W, O5W–O10W– O29–O3W, and O8W–O7W–O3W–O29 groups and the distances from three cap positions to the corresponding side planes are 1.6447 Å, 1.2126 Å and 1.7779 Å, respectively (Figure 2i, S2b). Notably, the O5W–O7W–O3W group and the O8W–O10W–O29 group define two bottom faces of the trigonal prism.

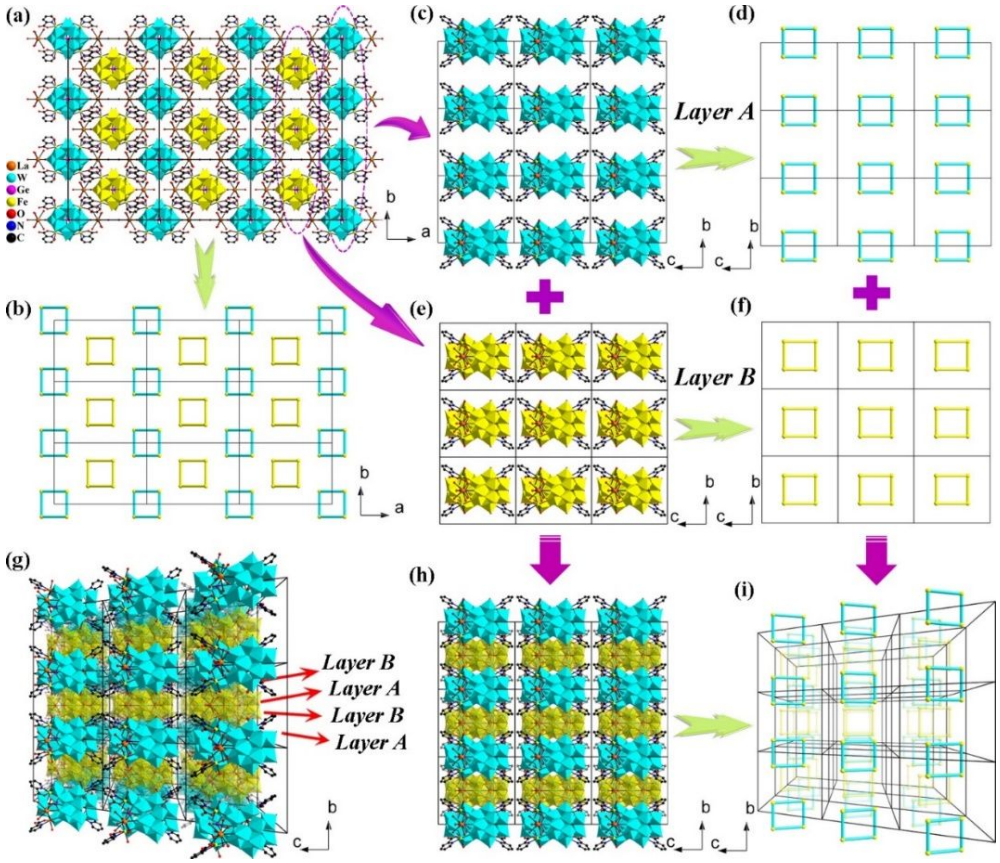

Figure S3. (a) Space packing for **1** with a regular –ABAB– fashion in ab plane. (b) Simplified packing for **1**. (c) Layer A in bc plane. (d) Simplified layer A. (e) Layer B in bc plane. (f) Simplified layer B. (g-h) Representations of 3D stacking for **1** in bc plane. (i) Simplified 3D stacking for **1** in bc plane.

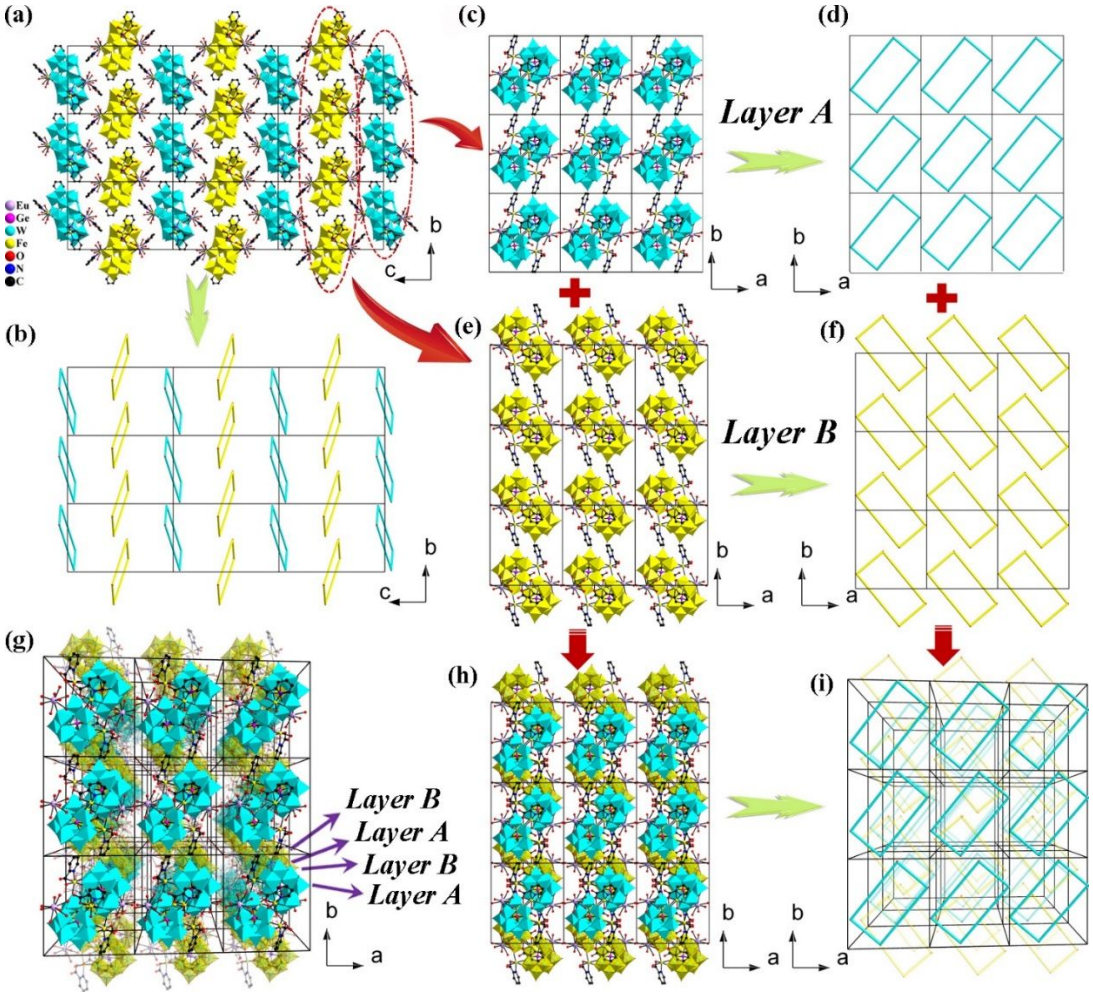

Figure S4. (a) Space packing for **10** with a regular –ABAB–fashion in ab plane. (b) Simplified packing for **10**. (c) Layer A in bc plane. (d) Simplified layer A. (e) Layer B in bc plane. (f) Simplified layer B. (g-h) Representations of 3D stacking for **10** in bc plane. (i) Simplified 3D stacking for **10** in bc plane.

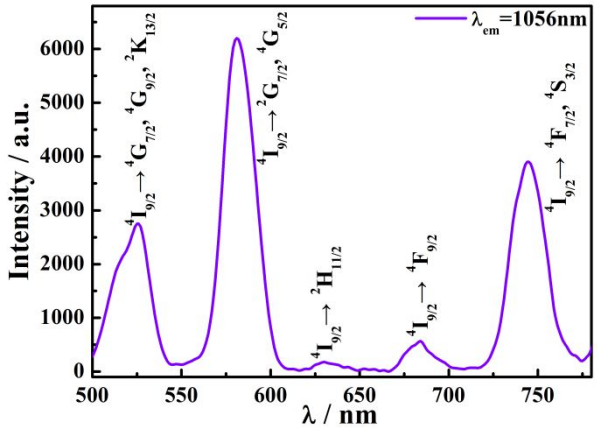

Figure S5. Solid-state excitation spectrum for **3** (λ_{em} = 1056 nm) at room temperature.

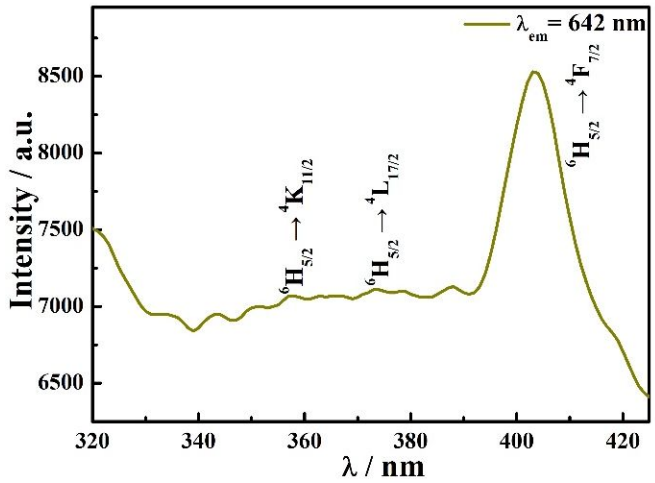

Figure S6. Solid-state excitation spectrum for **4** (λ_{em} = 642 nm) at room temperature.

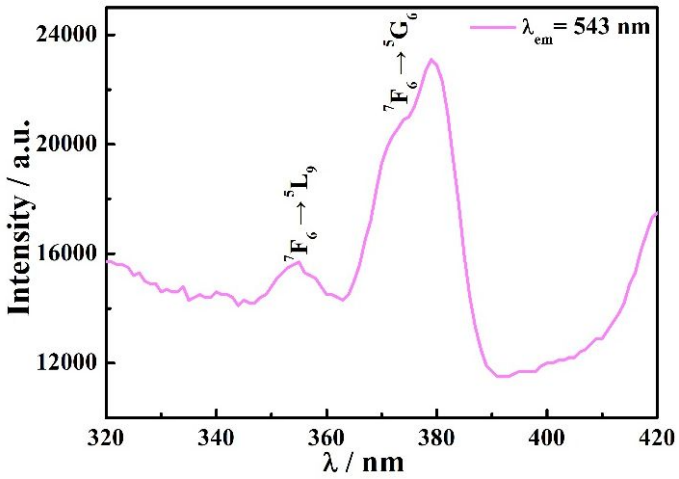

Figure S7. Solid-state excitation spectrum for **6** (λ_{em} = 543 nm) at room temperature.

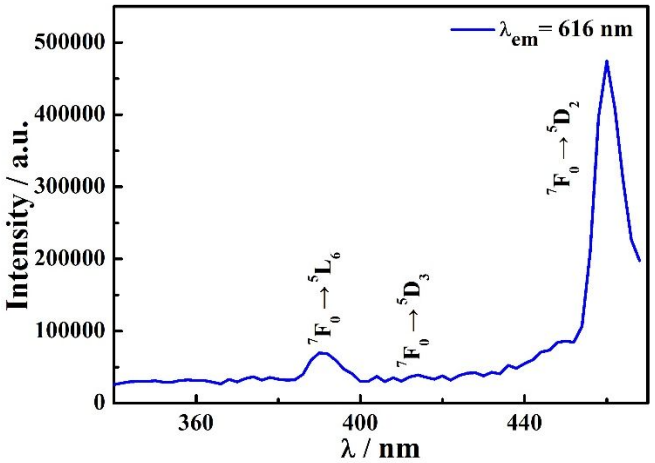

Figure S8. Solid-state excitation spectrum for **10** (λ_{em} = 616 nm) at room temperature.

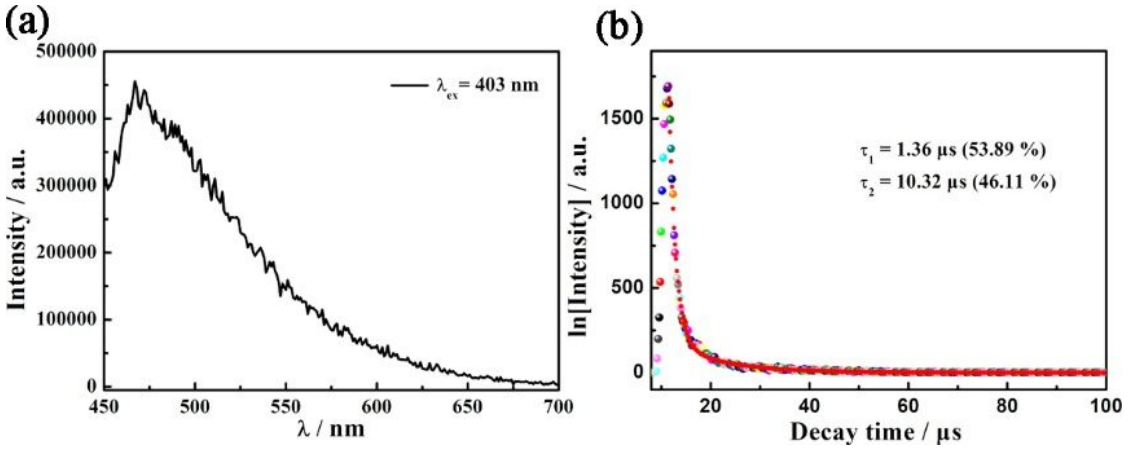

Figure S9. (a) Solid-state emission spectrum for $K_8[\gamma\text{-}GeW_{10}O_{36}]\cdot 6H_2O$ (λ_{ex} = 403 nm) at room temperature. (b) Luminescence decay profile for $K_8[\gamma\text{-}GeW_{10}O_{36}]\cdot 6H_2O$ taken through supervising 470 nm emission.

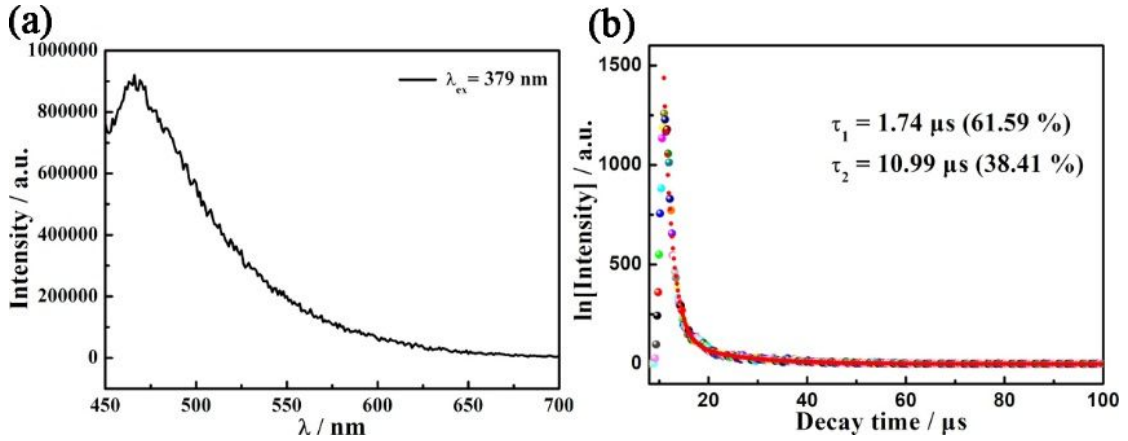

Figure S10. (a) Solid-state emission spectrum for $K_8[\gamma\text{-}GeW_{10}O_{36}]\cdot 6H_2O$ (λ_{ex} = 379 nm) at room temperature. (b) Luminescence decay profile for $K_8[\gamma\text{-}GeW_{10}O_{36}]\cdot 6H_2O$ taken through supervising 470 nm emission.

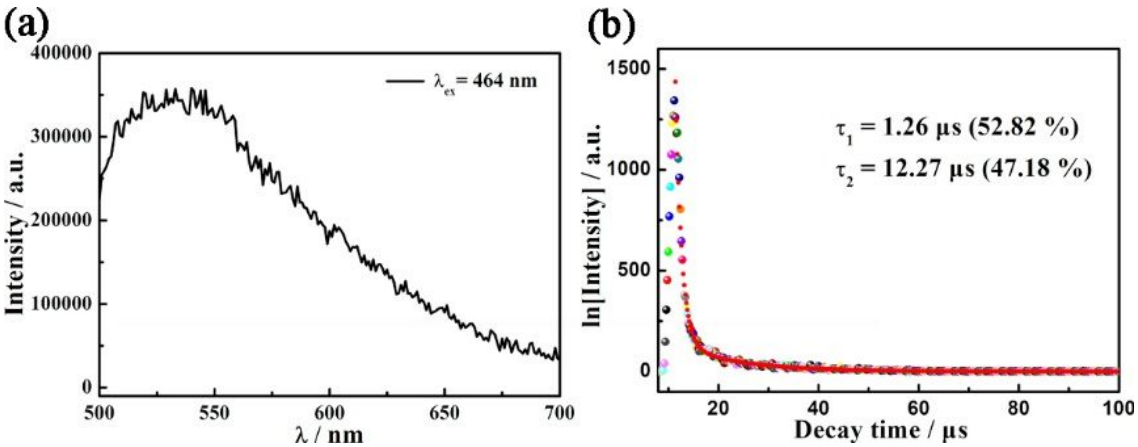

Figure S11. (a) Solid-state emission spectrum for $K_8[\gamma\text{-}GeW_{10}O_{36}]\cdot 6H_2O$ (λ_{ex} = 464 nm) at room temperature. (b) Luminescence decay profile for $K_8[\gamma\text{-}GeW_{10}O_{36}]\cdot 6H_2O$ taken through supervising 530 nm emission.

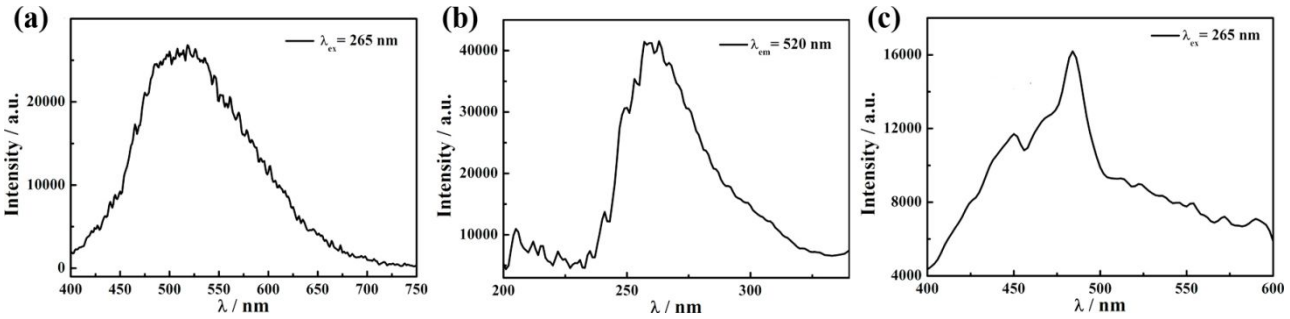

Figure S12. (a) Solid-state emission spectra for $K_8[\gamma\text{-}GeW_{10}O_{36}]\cdot 6H_2O$ (λ_{ex} = 265 nm) at room temperature. (b) Solid-state excitation spectrum for $K_8[\gamma\text{-}GeW_{10}O_{36}]\cdot 6H_2O$ (λ_{ex} = 520 nm) at room temperature. (c) Solid-state emission spectrum for Hpic ligand (λ_{ex} = 265 nm) at room temperature.

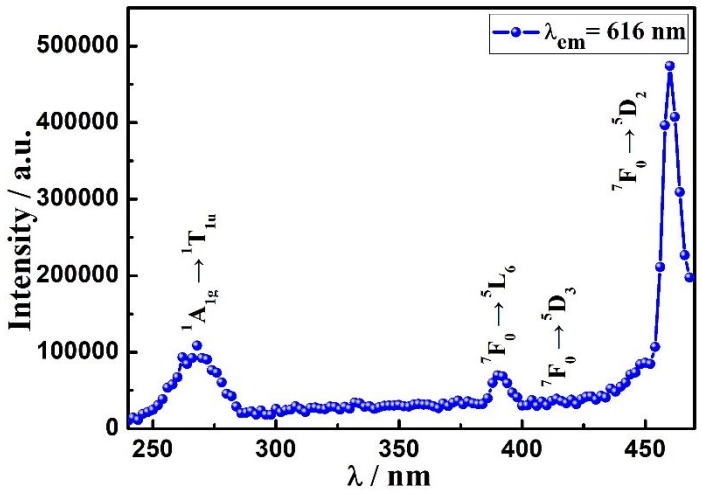

Figure S13. Excitation spectrogram for **10** (λ_{em} = 616 nm).

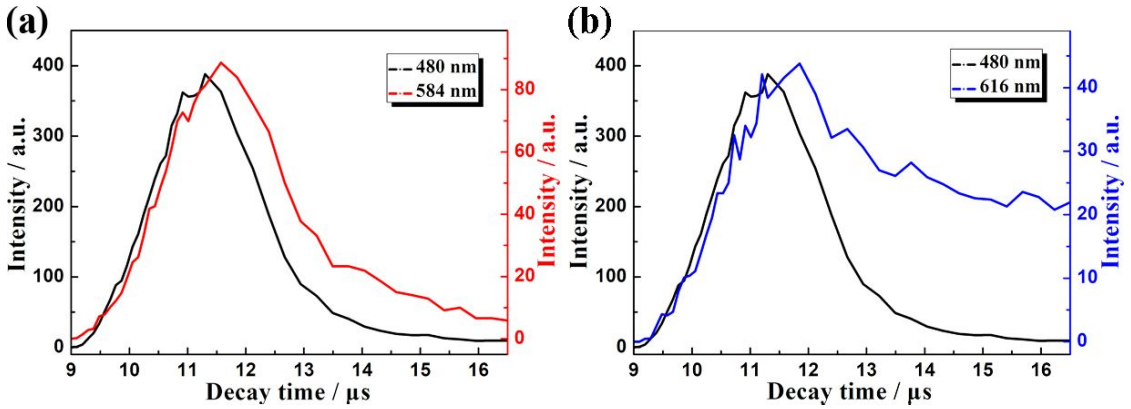

Figure S14. (a) The variation tendency of the intensity of emission peaks at 480 nm and 584 nm in the decay time range of 9.0 to 16.5 μs. (a) The variation tendency of the intensity of emission peaks at 480 nm and 616 nm in the decay time range of 9.0 to 16.5 μs.

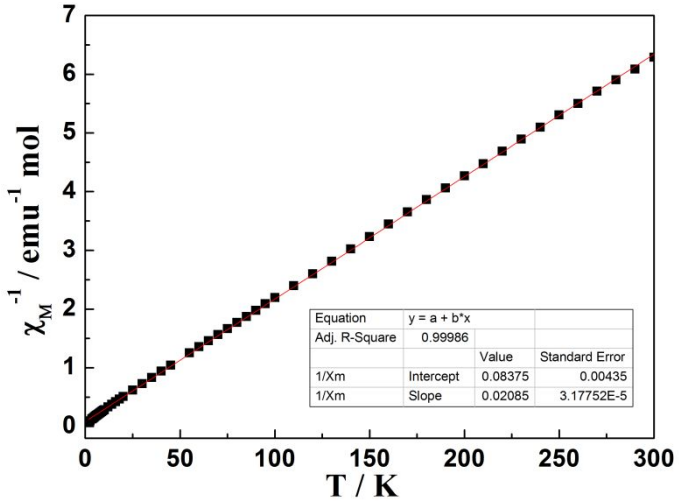

Figure S15. Temperature evolution of the inverse magnetic susceptibility for **7** between 0 and 300 K. The red solid line was generated from the best fit by the Curie-Weiss expression.

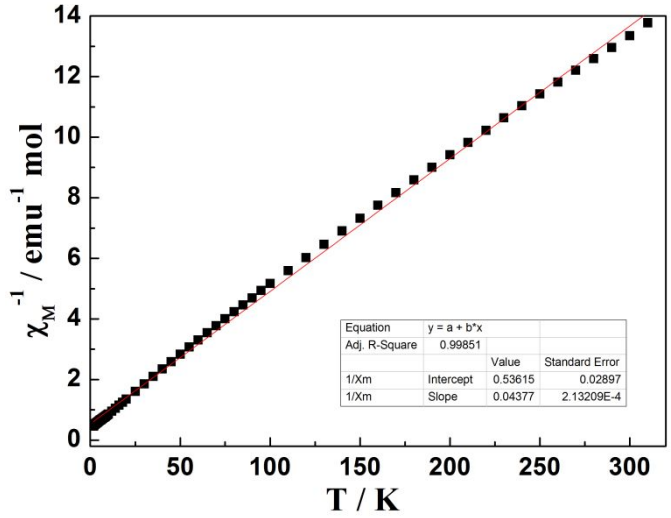

Figure S16. Temperature evolution of the inverse magnetic susceptibility for **10** between 0 and 300 K. The red solid line was generated from the best fit by the Curie-Weiss expression.

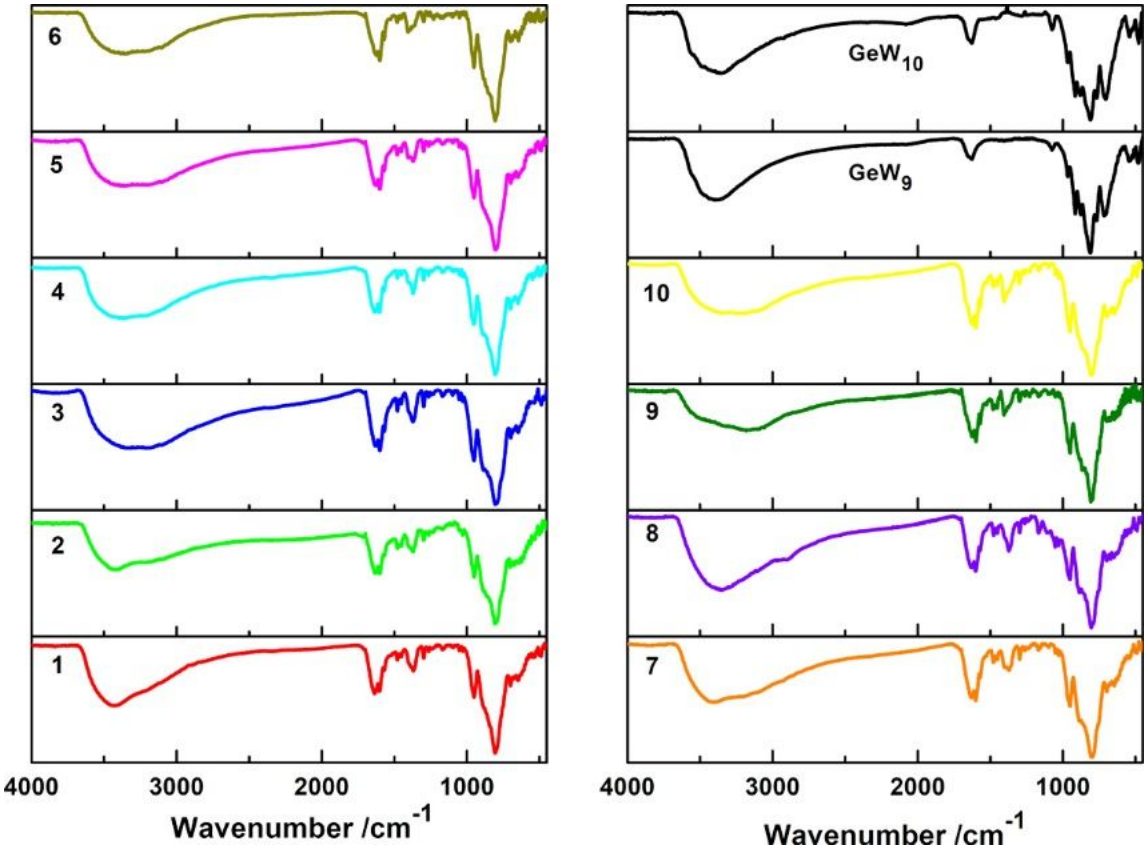

Figure S17. IR spectra of **1–10**, $K_8Na_2[A\text{-}\alpha\text{-}GeW_9O_{34}]\cdot 25H_2O$ and $K_8[\gamma\text{-}GeW_{10}O_{36}]\cdot 6H_2O$.

IR spectra

The IR spectra of **1–10** in the range of 4000–400 cm^{-1} have been recorded using solid samples palletized with KBr (Figure S17). Four characteristic peaks at 953, 806, 695 and 643 cm^{-1} are respectively attributed to $\nu(W\text{-}O_t)$, $\nu(Ge\text{-}O)$, $\nu(W\text{-}O_b)$ and $\nu(W\text{–}O_c)$ of the GT fragments. In addition, the absorption bands at 1638–1021 cm^{-1} can be regarded as characteristic peaks of pic ligands. Furthermore, as a rule, the carboxylic group is anticipated to show intense absorption bands from asymmetric (1640–1520 cm^{-1}) and symmetric (1480–1340 cm^{-1}) stretching vibrations. Obviously, the absorption bands observed at 1602–1595 cm^{-1} and 1411–1369 cm^{-1} are attributed to the asymmetric [$\nu_{as}(CO^{2-})$] and symmetric [$\nu_{sy}(CO^{2-})$] stretching vibrations of carboxylic groups of pic ligands, respectively.[1-2] In the high wavenumber region, the broad absorption band at around 3250 cm^{-1} can be regarded as a feature of the lattice and coordinated water molecules.

1 An H. Y.; Han Z. B.; Xu T. Q. Three-dimensional architectures based on lanthanide-substituted double Keggin-type polyoxometalates and lanthanide cations or lanthanide-organic complexes. *Inorg. Chem.* **2010**, *49*, 11403-11414;

2 Li C. H.; Huang K. L.; Chi Y. N.; Liu X.; Han Z. G.; Shen L.; Hu C. W. Lanthanide-organic cation frameworks with zeolite gismondine topology and large cavities from intersected channels templated by polyoxometalate counterions. *Inorg. Chem*. **2009**, *48*, 2010-2017.

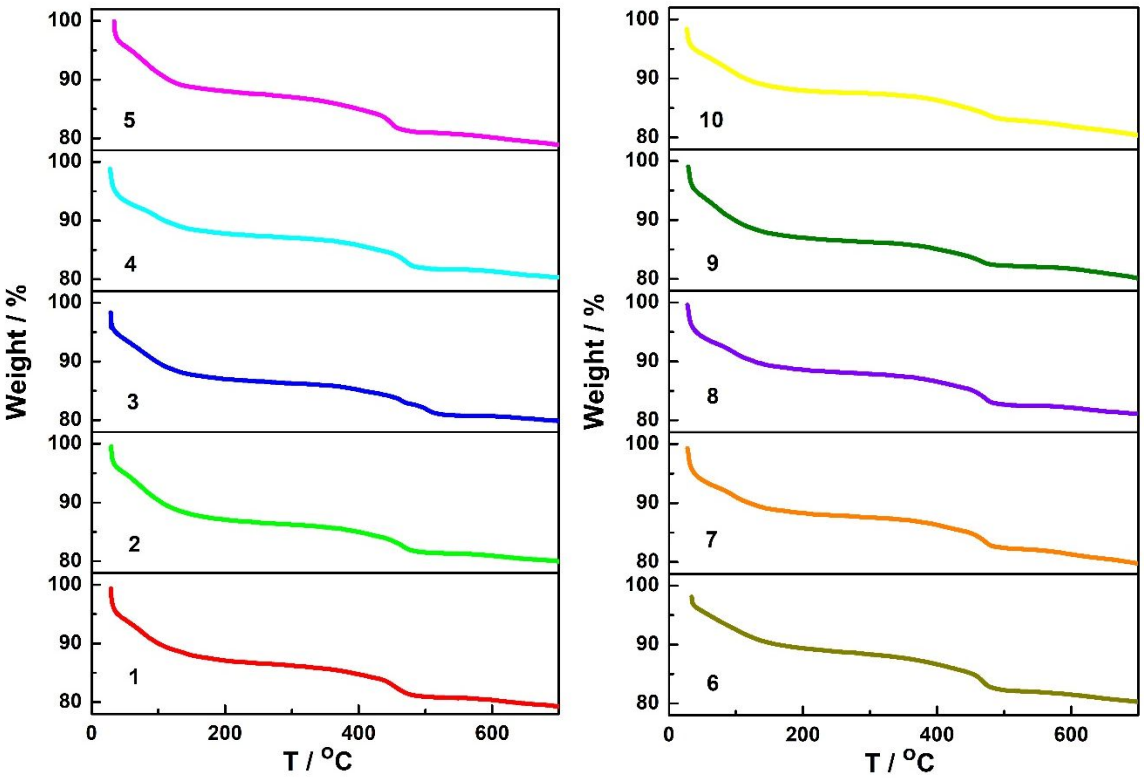

Figure S18. TG curves of **1–10**.

TG Analyses

For the sake of exploring the thermal stability of **1–10**, TG measurements were carried out from 25 to 700 °C under a N_2 atmosphere at a heating rate of 10 °C min^{-1}. The TG curves suggest that **1–9** undergo a two-step weight loss (Figure S18). For **1–9**, the first weight loss from 25 to 320 °C of 13.95 % (calcd. 14.27 %) for **1**, 13.90 % (calcd. 14.26 %) for **2**, 13.82 % (calcd. 14.25 %) for **3**, 13.05 % (calcd. 14.22%) for **4**, 13.24 % (calcd. 14.19 %) for **5**, 12.65 % (calcd. 14.19 %) for **6**, 12.85 % (calcd. 14.17 %) for **7**, 13.89 % (calcd. 14.15 %) for **8** and 13.45 % (calcd. 14.15 %) for **9** is attributed to the liberation of thirty-four lattice water molecules, twenty coordinate water molecules and the dehydration of two protons. The first weight loss 13.88 % (calcd. 14.65 %) from 25 to 320 °C for **10** is attributed to the liberation of thirty-six lattice water molecules, twenty coordinate water molecules and the dehydration of two protons. Upon heating to 700 °C, the second weight loss of 20.54 % (calcd. 21.36 %) for **1**, 20.00 % (calcd. 21.35 %) for **2**, 20.10 % (calcd. 21.33 %) for **3**, 19.19 % (calcd. 21.29 %) for **4**, 21.11 % (calcd. 21.25 %) for **5**, 19.66 % (calcd. 21.24 %) for **6**, 19.49 % (calcd. 21.22 %) for **7**, 19.77 % (calcd. 21.18 %) for **8** and 20.27 % (calcd. 21.19 %) for **9** is attributed to four pic ligands. Upon heating to 700 °C, the second weight loss of 19.91 % (calcd. 21.69 %) for **10** is attributed to four pic ligands.

Table S1. Crystallographic Data and Structure Refinements for 1–10.

	1	**2**	**3**	**4**	**5**
Empirical formula	$C_{24}H_{126}Ge_2Fe_4La_2N_4O_{134}W_{20}$	$C_{24}H_{126}Ge_2Fe_4Ce_2N_4O_{134}W_{20}$	$C_{24}H_{126}Ge_2Fe_4Nd_2N_4O_{134}W_{20}$	$C_{24}H_{126}Ge_2Fe_4Sm_2N_4O_{134}W_{20}$	$C_{24}H_{126}Ge_2Fe_4Gd_2N_4O_{134}W_{20}$
Formula weight	6938.68	6941.10	6949.34	6961.56	6975.36
Crystal system	Monoclinic	Monoclinic	Monoclinic	Monoclinic	Monoclinic
Space group	*C*2/m	*C*2/m	*C*2/m	*C*2/m	*C*2/m
a, Å	27.0401(6)	26.9373(11)	26.9043(8)	26.8026(6)	26.8102(5)
b, Å	14.8180(3)	14.7422(6)	14.7275(4)	14.6343(3)	14.6561(3)
c, Å	20.1643(8)	20.1339(16)	20.1635(5)	20.1356(4)	20.1777(7)
α, deg	90	90	90	90	90
β, deg	124.3240(10)	124.2020(10)	124.1850(10)	124.0180(10)	124.0330(10)
γ, deg	90	90	90	90	90
V, Å^{-3}	6672.5(3)	6612.7(7)	6609.1(3)	6546.3(2)	6570.5(3)
Z	2	2	2	2	2
μ, mm^{-1}	18.773	18.985	19.902	19.379	19.424
F(000)	6264	6268	6276.0	6284.0	6292.0
D_c, g cm^{-3}	3.454	3.486	3.492	3.532	3.526
T, K	150	150	150	150	150
Limiting indices	$-32 \le h \le 32$ $-17 \le k \le 17$ $-24 \le l \le 24$	$-32 <= h <= 32$ $-17 \le k \le 17$ $-24 <= l <= 24$	$-32 <= h <= 26$ $-17 \le k \le 17$ $-24 <= l <= 24$	$-31 <= h <= 29$ $-17 \le k \le 17$ $-24 <= l <= 23$	$-31 \le h \le 31$ $-16 \le k \le 17$ $-23 \le l \le 24$
Reflections collected/unique	38658 / 6147	29903 / 6081	30979 / 6081	29555 / 6014	41430 / 6046
R_{int}	0.0458	0.0501	0.0357	0.0604	0.0624
Data/restrains/parameters	6147 / 12 / 385	6081 / 0 / 389	6081 / 0 / 388	6014 / 13 / 388	6046 / 0 / 388
GOF on F^2	1.040	1.038	1.037	0.989	1.043
R_1, wR_2 ($I>2\sigma(I)$)[a]	0.0292, 0.0791	0.0266, 0.0689	0.0244, 0.0627	0.0320, 0.0679	0.0216, 0.0529
R_1, wR_2 (all data)	0.0306, 0.0801	0.0293, 0.0702	0.0263, 0.0638	0.0429, 0.0715	0.0252, 0.0539
	6	**7**	**8**	**9**	**10**
Empirical formula	$C_{24}H_{126}Ge_2Fe_4Tb_2N_4O_{134}W_{20}$	$C_{24}H_{126}Ge_2Fe_4Dy_2N_4O_{134}W_{20}$	$C_{24}H_{126}Ge_2Fe_4Tm_2N_4O_{134}W_{20}$	$C_{24}H_{126}Ge_2Fe_4Er_2N_4O_{134}W_{20}$	$C_{24}H_{130}Ge_2Fe_4Eu_2N_4O_{136}W_{20}$
Formula weight	6978.70	6985.86	6998.72	6995.18	7000.81
Crystal system	Monoclinic	Monoclinic	Monoclinic	Monoclinic	Monoclinic
Space group	*C*2/m	*C*2/m	*C*2/m	*C*2/m	*P*2(1)/*c*
a, Å	26.8034(10)	26.838(2)	26.8454(7)	26.9313(8)	15.2869(4)
b, Å	14.6355(6)	14.6163(12)	14.6001(4)	13.8212(5)	16.7796(4)
c, Å	20.1830(7)	20.215(3)	20.2286(5)	20.2797(8)	25.9984(6)
α, deg	90	90	90	90	90
β, deg	123.9320(10)	123.898(2)	124.0100(10)	123.0180(10)	97.0860(10)
γ, deg	90	90	90	90	90
V, Å^{-3}	6569.1(4)	6582.0(12)	6572.3(3)	6329.5(4)	6617.9(3)
Z	2	2	2	2	2
μ, mm^{-1}	19.495	19.517	19.759	20.441	19.232
F(000)	6216	6300.0	6312.0	6308.0	6328.0
D_c, g cm^{-3}	3.428	3.525	3.537	3.670	3.513
T, K	150	150	150	150	150
Limiting indices	$-31 \le h \le 31$ $-14 \le k \le 17$ $-24 \le l \le 23$	$-26 \le h \le 32$ $-17 \le k \le 15$ $-24 \le l \le 24$	$-26 \le h \le 32$ $-17 \le k \le 15$ $-24 \le l \le 24$	$-32 \le h \le 32$ $-16 \le k \le 16$ $-19 \le l \le 24$	$-18 \le h \le 18$ $-20 \le k \le 19$ $-31 \le l \le 31$
Reflections collected/unique	22669 / 6038	26121 / 6055	23204 / 5989	24940 / 5712	69954 / 11459
R_{int}	0.0461	0.0619	0.0407	0.0530	0.0468
Data/restrains/parameters	6038 / 0 / 388	6055 / 55 / 425	5989 / 0 / 384	5712 / 6 / 376	11459 / 0 / 742
GOF on F^2	1.020	1.063	1.069	1.056	1.038
R_1, wR_2 ($I>2\sigma(I)$)[a]	0.0372, 0.0920	0.0627, 0.1755	0.0326, 0.0798	0.0402, 0.0927	0.0279, 0.0621
R_1, wR_2 (all data)	0.0416, 0.0944	0.0704, 0.1816	0.0381, 0.0819	0.0576, 0.0988	0.0308, 0.0633

Table S2. Bond Valence Sum (BVS) Calculations of All the W, Fe, Ge and Ln Atoms in **1** and **10**.

Atom	La	W1	W2	W3	W4	W5	W6	Ge	Fe

BVS(**1**)	3.18	6.05	6.15	6.18	6.18	6.13	6.08	4.03	2.95

Atom	Eu	W1	W2	W3	W4	W5	W6
BVS(**10**)	3.07	6.12	6.21	6.14	6.14	6.13	6.13
Atom	W7	W8	W9	W10	Fe1	Fe2	Ge1
BVS(**10**)	6.11	6.10	6.13	6.11	3.11	3.10	4.03